Journal of Alloys and Compounds 590 (2014) 50–60

Contents lists available at ScienceDirect

Journal of Alloys and Compounds

journal homepage: www.elsevier.com/locate/jalcom

Stability, elastic properties and electronic structures of the stable Zr–Al intermetallic compounds: A first-principles investigation

Y.H. Duan [a,b,*], B. Huang [a], Y. Sun [a], M.J. Peng [a], S.G. Zhou [a]

[a] School of Material Science and Engineering, Kunming University of Science and Technology, Kunming 650093, China
[b] Key Lab of Advance Materials in Rare & Precious and Nonferrous Metals, Ministry of Education, China, Kunming 650093, China

ARTICLE INFO

Article history:
Received 31 October 2013
Received in revised form 9 December 2013
Accepted 9 December 2013
Available online 16 December 2013

Keywords:
First-principles
Zr–Al compounds
Phase stability
Elastic properties
Electronic structures

ABSTRACT

To better clarify and understand the phase stability and elastic properties of stable Zr–Al binary intermetallic compounds, the structural properties, phase stability, elastic properties, and electronic structures of these compounds in Zr–Al system have been systematically investigated by using first-principles calculations. The calculated equilibrium structures and enthalpies of formation in present work are in good agreement with the available experimental and other theoretical data, and the results of enthalpies of formation show that $ZrAl_2$ is the most stable. The elastic properties, including elastic constants, Poisson's ratio and anisotropy index, and Debye temperatures were also investigated. It is found that ZrAl is the most anisotropic in Zr–Al binary compounds. Furthermore, the electronic structures were discussed to reveal the bonding characteristics of the compounds.

1. Introduction

Due to good mechanical properties at high temperature combined with low absorption cross-section for thermal neutrons, zirconium–aluminum alloys have drawn comprehensive attention in potential structure materials in thermal nuclear reactors [1–3]. Amount of work has been investigated on the Zr–Al alloys in respects of amorphisation [4], nano-phase formation [5], formation of several metastable phases [6] and also making zirconium based pressure tubes with aluminum lining [7]. As reviewed by Murray et al. [8], the Al–Zr system is characterized by the presence of ten stable phases which are $ZrAl_3$, $ZrAl_2$, Zr_2Al_3, ZrAl, Zr_5Al_4, Zr_4Al_3, Zr_3Al_2, Zr_5Al_3, Zr_2Al and Zr_3Al. The getter potentialities, elastic modulus and combustion synthesis of partial Zr–Al intermetallic compounds (mainly focused on $ZrAl_2$ and $ZrAl_3$) have been investigated [9–11]. The existence of the large number of observed Zr–Al phases is attributed to the fact that the heats of formation for Zr_xAl_{1-x} (x = 0.25–0.75) fall on a nearly straight line by using the full-potential linearized augmented Slater-type orbital (LASTO) method [12]. The main contribution to the electric field gradient of Laves phase $ZrAl_2$ with $MgZn_2$-type structure comes from the Zr and Al's p electrons [13]. Moreover, the results of mechanical properties of Laves phases $ZrAl_2$ and $HfAl_2$ with C14-type structure show that the anisotropy degree of $HfAl_2$ is slightly larger than that of $ZrAl_2$ and $ZrAl_2$ is brittle and isotopic in shear [14]. The order of relative stabilities of $L1_2$, $D0_{22}$, and $D0_{23}$ structure in the $ZrAl_3$ intermetallic compound are $D0_{23} > D0_{22} > L1_2$ [15]. By performed nuclear magnetic resonance measurements, $ZrAl_3$ is more stable than $HfAl_3$ with respect to the $D0_{23}$ structure [16]. Elastic constants of $D0_{23}$-$ZrAl_3$ single crystal have been measured from the velocity of ultrasonic waves and the estimated Poisson's and Debye temperature of $D0_{23}$-$ZrAl_3$ are 0.18 and 577 K, respectively [17]. However, there is a lack of the systematical calculations of phase stability, elastic properties and electronic structure for these ten compounds.

The fundamental understanding of both the mechanical properties and phase stability of intermetallics provided by the results of quantum–mechanical electronic structure calculations have been significantly improved over the last 20 years. Ab initio or first-principles methods based upon electronic density-functional theory (DFT) [18] have been employed to derive a number of bulk and defect properties including enthalpy of formation, the relative stability of competing structures, elastic constants, lattice parameters, and the energies associated with point and planar defects [19,20].

In this work, the first-principles calculations were performed to better clarify and understand the phase stability and elastic properties of Zr–Al binary intermetallic compounds consisting of enthalpy of formation, elastic constants, Young's modulus E, shear modulus G, bulk modulus B, Poisson's ratio v and anisotropy index A. Based on the calculated elastic constants and modulus, the

* Corresponding author at: School of Material Science and Engineering, Kunming University of Science and Technology, Kunming 650093, China. Tel./fax: +86 871 65136698.
E-mail address: duanyh@kmust.edu.cn (Y.H. Duan).

0925-8388/$ - see front matter © 2013 Elsevier B.V. All rights reserved.
http://dx.doi.org/10.1016/j.jallcom.2013.12.079

cDebye temperature were also investigated. Further, the electronic structures were discussed.

2. Computational method

All calculations were performed by using the first principles calculations based on density functional theory (DFT) implemented in CASTEP (Cambridge sequential total energy package) code [21]. Ultra-soft pseudo-potentials were employed to indicate the interactions between ionic core and valence electrons. The exchange correlation energy was described by using the generalized gradient approximation (GGA) with the Perdew–Burke–Ernzerhof (PBE) parameterization [22]. Valence electrons included in this study for distinct atoms were Al $3s^2 3p^1$ and Zr $4s^2 4p^6 4d^2 5s^2$. The Monkhorst–Pack scheme was used for k point sampling in the first irreducible Brillouin zone (BZ). The k points separation in the Brillouin zone of the reciprocal space were $18 \times 18 \times 18$, $12 \times 12 \times 6$, $15 \times 15 \times 12$, $12 \times 8 \times 16$, $14 \times 4 \times 12$, $12 \times 12 \times 16$, $10 \times 10 \times 12$, $12 \times 12 \times 16$, $8 \times 8 \times 20$, $18 \times 18 \times 12$, $18 \times 18 \times 18$, $18 \times 18 \times 12$ for Al (fcc), $ZrAl_3$, $ZrAl_2$, Zr_2Al_3, ZrAl, Zr_5Al_4, Zr_4Al_3, Zr_3Al_2, Zr_5Al_3, Zr_2Al, Zr_3Al, α-Zr (hcp) respectively. The cutoff energy for plane wave expansions was determined as 400 eV after convergence tests. The separation of the reciprocal space was around 0.01 $Å^{-1}$ and the SCF (self-consistent field) tolerance was set as 5×10^{-7} eV/atom. The crystal structures of ten stable Zr–Al compounds are shown in Fig. 1. The lattice parameters and atomic coordinates are tabulated in Tables 1 and 2, respectively.

3. Results and discussion

3.1. Structural properties

In present work, the initial crystal structures have been built based upon the experimental crystallographic data of Al, α-Zr and ten types of Zr–Al intermetallic compounds in Zr–Al binary alloys [23,34], then the lattice parameters and internal coordinates of these compounds were optimized by using first-principle calculations. The optimized lattice parameters are listed in Table 1 compared to the available experimental data. The average deviation between the experiments and the calculated values is about 1%, which is expected for the first-principles calculations using GGA. The calculated lattice parameters of Al, α-Zr and Zr–Al intermetallic compounds agree very well with the available experimental data. Table 2 lists detailed comparisons between calculations and measurements for atomic coordinates. For these ten phases, the agreement between experiment and theory can be considered as only reasonable. These agreements of optimized lattice parameters and atomic coordinates with the experimental values provide a confirmation that the computational methodology utilized in this work is suitable and reliable.

3.2. Enthalpies of formation and phase stability

In order to estimate the structural stability of these Zr–Al intermetallic compounds, the cohesive energy (E_c) and enthalpy of formation (ΔH) were calculated.

The cohesive energy is defined as the work which is needed when the crystal is decomposed into isolated atoms. The more negative cohesive energy indicates the released energy is larger in the process of formation of the compound. The cohesive energy (E_c) per atom of Zr_xAl_y is calculated by the following expressions:

$$E_c = [E_{\text{total}} - (xE_{\text{Zr}} + yE_{\text{Al}})]/(x+y) \quad (1)$$

where E_{Zr} and E_{Al} are the total energies of isolated Zr and Al atom, respectively; x, y are the number of atoms in the chemical formula of Zr_xAl_y. E_{total} is the total energy of Zr_xAl_y.

Enthalpy of formation of Zr_xAl_y is defined as the difference in total energy of the compound and the energies of its constituent elements in their stable states:

$$\Delta H = \left[E_{total} - (xE_{Zr}^{bulk} + yE_{Al}^{bulk})\right] \Big/ (x+y) \quad (2)$$

where E_{Zr} and E_{Al} are the total energies of isolated Zr and Al atoms, respectively; E_{total} is the total energy of Zr_xAl_y, E_{Zr}^{bulk} and E_{Al}^{bulk} are the total energy of a Zr atom and an Al atom in the bulk state. Negative enthalpy of formation usually means an exothermic process, and a more negative enthalpy of formation corresponds to a better phase stability.

The calculated cohesive energies and enthalpies of formation of the ten binary compounds together with their available experimental and other theoretical calculated data [15,38–41] are tabulated in Table 3 and plotted in Fig. 2 (enthalpies of formation), and in Fig. 2 the present calculated and other theoretical calculated values are plotted in the x- and y-axis, respectively. The enthalpies of formation from first-principles calculations compare favorably with ab initio approach (Fig. 2(a)) and CALPHAD approach (Fig. 2(b)) for most compounds. In Fig. 2, the solid line implies a perfect agreement between the present calculated and other theoretical calculated values, and two dashed lines are represented an error bar of ±2.5 kJ/mol (Note: in this paper, the unit kJ/mol means kJ/mole of atoms.). With regard to all the stable compounds in the Zr–Al binary system, the first-principles calculated enthalpies of formation agree well with those from the ab initio approach and CALPHAD approach with differences less than 2.5 kJ/mol.

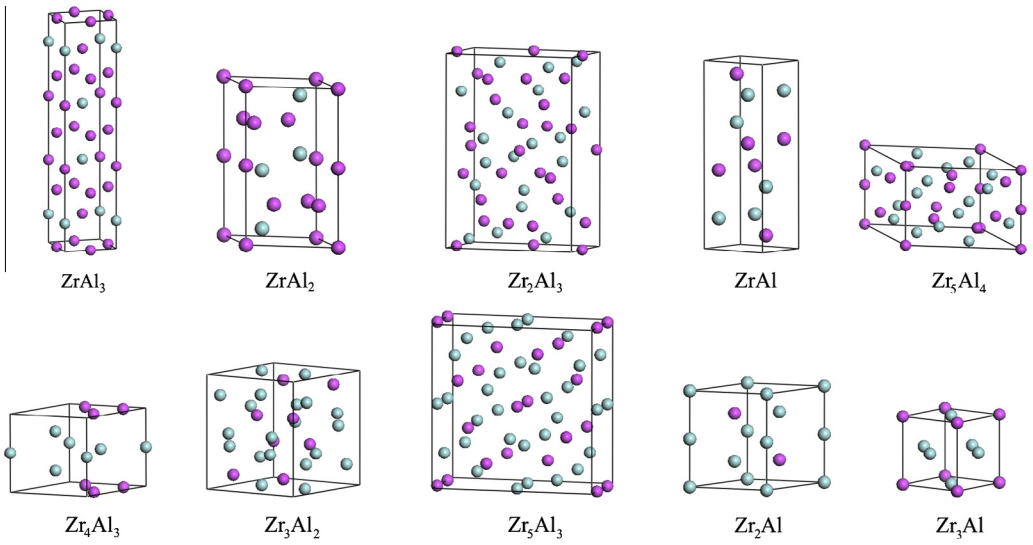

Fig. 1. The crystal structures of ten stable Zr–Al compounds. The purple balls and cyan balls represent Al and Zr, respectively. (For interpretation of the references to colour in this figure legend, the reader is referred to the web version of this article.)

Table 1
Calculated and experimental lattice parameters for Al, Zr and Zr–Al intermetallic compounds in Zr–Al binary alloys.

Phase	At% Zr	Space group	Pearson symbol	Lattice parameters (Å)			Refs.
				a	*b*	*c*	
Al	0.0	*Fm*-3*m*	cF4	4.049			Present
				4.049			[23]
$ZrAl_3$	25.0	*I*4/*mmm*	*tI*16	4.020		17.329	Present
				4.007		17.286	[24]
$ZrAl_2$	33.3	*P*6$_3$/*mmc*	*hP*12	5.297		8.780	Present
				5.281		8.742	[25]
Zr_2Al_3	40.0	*Fdd*2	*oF*40	9.648	13.936	5.599	Present
				9.617	13.934	5.584	[24]
				9.601	13.906	5.570	[26]
ZrAl	50.0	*Cmcm*	oC8	3.360	10.961	4.288	Present
				3.359	10.887	4.274	[27]
Zr_5Al_4	55.6	*P*6$_3$/*mcm*	*hP*18	8.462		5.793	Present
				8.432		5.791	[24]
Zr_4Al_3	57.1	*P*-6	hP7	5.449		5.394	Present
				5.433		5.390	[28]
Zr_3Al_2	60.0	*P*4$_2$/*mnm*	*tP*20	7.664		6.997	Present
				7.663		6.996	[24]
				7.630		6.998	[29]
Zr_5Al_3	62.5	I4/*mcm*	*tI*32	11.066		5.396	Present
				11.043		5.392	[24]
				11.049		5.396	[30]
Zr_2Al	66.7	P6$_3$/*mmc*	hP6	4.908		5.928	Present
				4.894		5.928	[31]
				4.882		5.918	[32]
Zr_3Al	75.0	*Pm*-3*m*	cP4	4.381			Present
				4.374			[32]
				4.372			[33]
α-Zr	100.0	*P*6$_3$/*mmc*	hP2	3.232		5.173	Present
				3.231		5.148	[34]

Fig. 3 plots calculated cohesive energies and enthalpies of formation as a function of the mole fraction of Zr. As can be seen in Table 3 and Fig. 3(a), the present calculated cohesive energies of Al, $ZrAl_3$ and Zr are −3.733 eV/atom, −5.137 eV/atom and −8.410 eV/atom, respectively, which are in good agreement with the reported −3.691 eV/atom, −5.241 eV/atom and -8.398 eV/atom for Al, $ZrAl_3$ and Zr [15]. From Fig. 3(a), we note that the cohesive energies of the intermetallic compounds in the Zr–Al system approximately have a linear declining trend with the increasing mole fraction of Zr. Zr_3Al possesses the most negative cohesive energy in these ten Zr–Al binary compounds, which indicates that the released energy in the process of formation of Zr_3Al compound is the largest.

For the considered Zr–Al system, more than one ordered binary compound are investigated. Eight compounds in the Zr–Al binary system are stable at low temperatures in the Zr–Al phase diagram except for Zr_5Al_4 and Zr_5Al_3 which are experimentally observed to be stable only at high temperatures. Our calculations of enthalpies of formation are illustrated a convex hull determined by five compounds in the Zr–Al system: $ZrAl_3$, $ZrAl_2$, Zr_2Al_3, Zr_4Al_3 and Zr_3Al. The convex hull is shown in Fig. 3(b). It is obvious, in Fig. 3(b), that the convex hull is asymmetric and inclined towards Al side with a maximum in enthalpy of formation at $ZrAl_2$. The deviations of the convex hull for ZrAl, Zr_2Al and Zr_3Al_2 are 1.0 kJ/mol, 1.5 kJ/mol and 3.5 kJ/mol, respectively. The energies lying of ZrAl and Zr_2Al close to the convex hull indicates that they are stable at experimentally temperatures. The stability of Zr_3Al_2 is hard to explain according to Fig. 3(b), however, the negative enthalpy of formation for Zr_3Al_2 (−38.262 kJ/mol) reveals the observed stability of Zr_3Al_2. The calculated enthalpies of formation for Zr_5Al_4 and Zr_5Al_3 lie above the convex hull by 5 kJ/mol in Fig. 3(b), and these two phases are experimentally observed to be stable at high temperatures.

The calculated enthalpies of formation for three compounds, which located at the bottom of the convex hull in Fig. 3(b), are −46.780 kJ/mol for $ZrAl_3$, −51.603 kJ/mol for $ZrAl_2$, and −49.867 kJ/mol for Zr_2Al_3, respectively. The most negative enthalpy of formation implies stronger Zr–Al bonds and better phase stability. $ZrAl_2$ has the most stability in the ten binary compounds in the Zr–Al system.

3.3. Elastic properties

The single-crystal elastic constants can be obtained by first-principles calculation by calculating the total energy as a function of appropriate lattice deformation. To calculate the elastic constants C_{ij}, a deformed cell is introduced. The elastic strain energy is given by fellow [42]:

$$U = \Delta E/V_0 = 1/2\sum_{i}^{6}\sum_{j}^{6} C_{ij}e_i e_j \quad (3)$$

where ΔE is the energy difference; V_0 is the volume of the original cell; C_{ij} is the elastic constants; e_i and e_j are strain.

The calculated elastic constants C_{ij} of the ten Zr–Al compounds together with the available theoretical data [17,43,44] are listed in Table 4. The mechanical stabilities of the ten compounds have been discussed on the basis of elastic constants. For various crystals, the elastic constants need to satisfy the generalized stability criteria: $C_{11} > 0$, $C_{44} > 0$, $C_{11} > C_{12}$, $C_{11} + 2C_{12} > 0$ for cubic crystals [45]; $C_{11} > 0$, $C_{44} > 0$, $C_{11} > C_{12}$, $(C_{11} + C_{12})C_{33} - 2C_{13}^2 > 0$ for hexagonal crystals [46]; $C_{11} > 0$, $C_{33} > 0$, $C_{44} > 0$, $C_{66} > 0$, $C_{11} > C_{12}$, $C_{11} + C_{33} - 2C_{13} > 0$, $2C_{11} + C_{33} + 2C_{12} + 4C_{13} > 0$ for tetragonal crystals [47]; $C_{11} > 0$, $C_{22} > 0$, $C_{33} > 0$, $C_{44} > 0$, $C_{55} > 0$, $C_{66} > 0$, $C_{11} + C_{22} - 2C_{12} > 0$, $C_{11} + C_{33} - 2C_{13} > 0$, $C_{22} + C_{33} - 2C_{23} > 0$, $C_{11} + C_{22} + C_{33} + 2C_{12} + 2C_{13} + 2C_{23} > 0$ for orthorhombic crystals [48].

It is obvious that, from Table 4, the elastic constants of the cubic crystal Zr_3Al satisfy the mechanical stability criteria with $C_{11} = 146.45 > 0$, $C_{44} = 75.67 > 0$, $C_{11} = 146.45 > C_{12} = 74.27$, $C_{11} + 2C_{12} = 294.99 > 0$. As for the four hexagonal crystals ($ZrAl_2$, Zr_5Al_4, Zr_4Al_3 and Zr_2Al), the elastic constants are consistent with the restrictions to hexagonal crystals. For the three tetragonal crystals ($ZrAl_3$, Zr_3Al_2 and Zr_5Al_3) and two orthorhombic crystals

Table 2
Calculated and experimental unit cell-internal parameters (Wyckoff positions) for Zr–Al intermetallic compounds in Zr–Al binary alloys.

Phase		Unit cell-internal parameters (Wyckoff positions)					
		Present work (x, y, z)			Experiment (x, y, z) [Ref.]		
$ZrAl_3$	Zr:4e	0.00000	0.00000	0.11820	0.00000	0.00000	0.11886 [35]
	Al1:4c	0.00000	0.50000	0.00000	0.00000	0.50000	0.00000
	Al2:4d	0.00000	0.50000	0.25000	0.00000	0.50000	0.25000
	Al3:4e	0.00000	0.00000	0.37442	0.00000	0.00000	0.37498
$ZrAl_2$	Zr:4f	0.33333	0.66667	0.06477	0.33333	0.66667	0.06533 [25]
	Al1:2a	0.00000	0.00000	0.00000	0.00000	0.00000	0.00000
	Al2:6h	0.82920	0.65840	0.25000	0.82800	0.65600	0.25000
Zr_2Al_3	Zr:16b	0.18277	0.05276	0.00000	0.18500	0.05200	0.00000 [26]
	Al1:8a	0.00000	0.00000	0.59987	0.00000	0.00000	0.62000
	Al2:16b	0.18170	0.11485	0.50000	0.18000	0.12500	0.50000
ZrAl	Zr:4c	0.00000	0.16120	0.25000	0.00000	0.16600	0.25000 [32]
	Al:4c	0.00000	0.42874	0.25000	0.00000	0.42400	0.25000
Zr_5Al_4	Zr1:4d	0.33333	0.66667	0.00000	0.33333	0.66667	0.00000 [36]
	Zr2:6g	0.29017	0.00000	0.25000	0.29000	0.00000	0.25000
	Al1:2b	0.00000	0.00000	0.00000	0.00000	0.00000	0.00000
	Al2:6g	0.62982	0.00000	0.25000	0.62000	0.00000	0.25000
Zr_4Al_3	Zr1:2h	0.33333	0.66667	0.26064	0.33333	0.66667	0.25000 [28]
	Zr2:1f	0.66667	0.33333	0.50000	0.66667	0.33333	0.50000
	Zr3:1b	0.00000	0.00000	0.50000	0.00000	0.00000	0.50000
	Al:3j	0.33331	0.16669	0.00000	0.33333	0.16667	0.00000
Zr_3Al_2	Zr1:4d	0.00000	0.50000	0.25000	0.00000	0.50000	0.25000 [29]
	Zr2:4f	0.34325	0.34325	0.00000	0.34000	0.34000	0.00000
	Zr3:4g	0.19942	0.80058	0.00000	0.20000	0.80000	0.00000
	Al:8j	0.12112	0.12112	0.21319	0.12500	0.12500	0.25000
Zr_5Al_3	Zr1:4b	0.00000	0.50000	0.25000	0.00000	0.50000	0.25000 [30]
	Zr2:16k	0.07965	0.21944	0.00000	0.07700	0.21800	0.00000
	Al1:4a	0.00000	0.00000	0.25000	0.00000	0.00000	0.25000
	Al2:8h	0.16273	0.66273	0.00000	0.16000	0.66000	0.00000
Zr_2Al	Zr1:2a	0.00000	0.00000	0.00000	0.00000	0.00000	0.00000 [37]
	Zr2:2d	0.33333	0.66667	0.75000	0.33333	0.66667	0.75000
	Al1:2c	0.33333	0.66667	0.25000	0.33333	0.66667	0.25000
Zr_3Al	Zr:3c	0.00000	0.50000	0.50000	0.00000	0.50000	0.50000 [37]
	Al:1a	0.00000	0.00000	0.00000	0.00000	0.00000	0.00000

Table 3
The calculated cohesive energies and a comparison of enthalpies of formation (ΔH) for Zr–Al intermetallic compounds in Zr–Al binary alloys obtained by various methods: ab intio calculations (at 0 K), experiment (at different temperatures), and CALPHAD (at 298.15 K or the standard enthalpy of formation) modeling of Zr–Al phase diagram.

Phase	E_c (eV/atom)	ΔH (kJ/mol)			
		Present	Ab initio [38]	Experiment	CALPHAD
Al	−3.733	0			
	−3.691 [15]				
$ZrAl_3$	−5.137	−46.780	−49.106	−48.4 ± 1.3 [39]	−48.50 [41]
	−5.241 [15]				
$ZrAl_2$	−5.494	−51.603	−53.327	−52.1 ± 1.6 [39]	−52.60 [41]
Zr_2Al_3	−5.721	−49.867	−51.649	−55 ± 4 [24]	−46.94 [40]
ZrAl	−6.037	−44.875	−46.163	−53 ± 4 [24]	−44.50 [40]
Zr_5Al_4	−6.192	−40.175	−42.002	−52 ± 4 [24]	−41.00 [40]
Zr_4Al_3	−6.296	−44.568	−47.555		−58.48 [41]
Zr_3Al_2	−6.336	−38.262	−39.298	−49 ± 4 [24]	−38.43 [40]
Zr_5Al_3	−6.401	−35.308	−37.599	−48 ± 4 [24]	−36.25 [40]
Zr_2Al	−6.539	−34.222	−36.753		−33.37 [40]
Zr_3Al	−6.791	−28.994	−31.088	−27.0 [40]	−36.16 [41]
α-Zr	−8.410	0			
	−8.398 [15]				

(Zr_2Al_3 and ZrAl), all the elastic constants meet the corresponding crystal's mechanical stability criteria. The results reveal that all the ten Zr–Al binary compounds are mechanically stable. Furthermore, it is well known that the elastic constant C_{44} is the most significant parameter which indirectly determining the indentation hardness of a solid [49]. A large C_{44} implies a strong resistance to shear in the (100) plane. The highest C_{44} for $ZrAl_2$ than that for the other Zr–Al compounds means that its ability to resist shear distortion in the (100) plane is the strongest.

The polycrystalline bulk modulus B, shear modulus G, Young's modulus E and Poisson's ratio v have been obtained in terms of their elastic constants, and the results are tabulated in Table 5.

The calculated bulk moduli of the ten binary compounds together with their available theoretical calculated data [38] are plotted in Fig. 4. With regard to all the compounds in the Zr–Al binary system, the first-principles calculated bulk moduli agree well with those from the ab initio approach with differences less than 2.5 GPa. As a fundamental physical property of a solid, bulk modu-

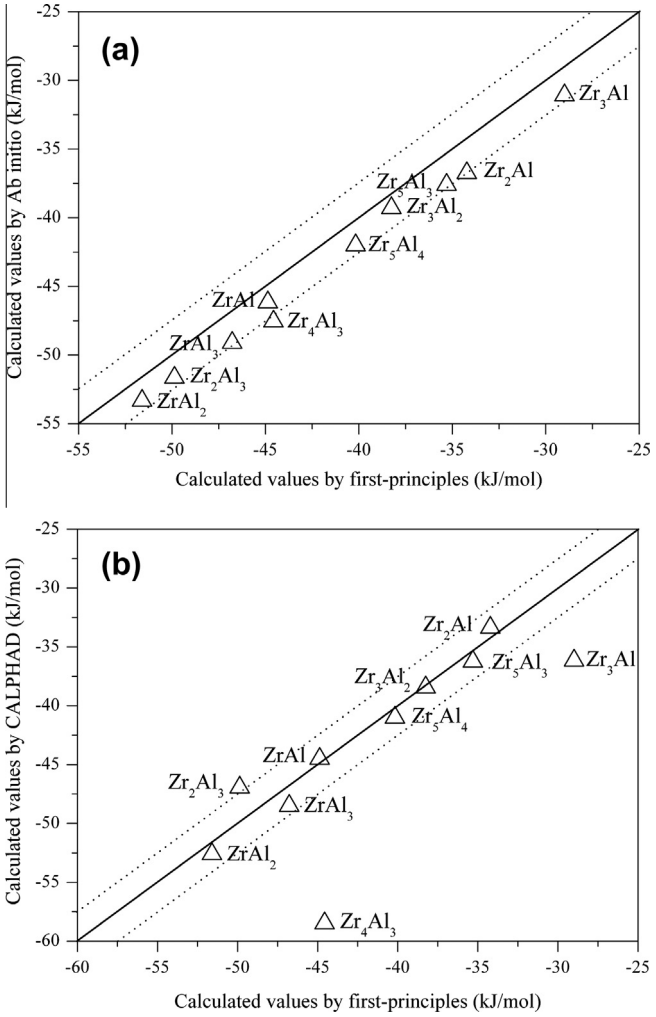

Fig. 2. Comparison of calculated enthalpies of formation in this work for the binary intermetallic compounds in the Zr–Al systems with the calculated values by ab initio calculations (a) and CALPHAD (b). The solid line shows unity ($y = x$) while the dotted lines present an error range of ±2.5 kJ/mol.

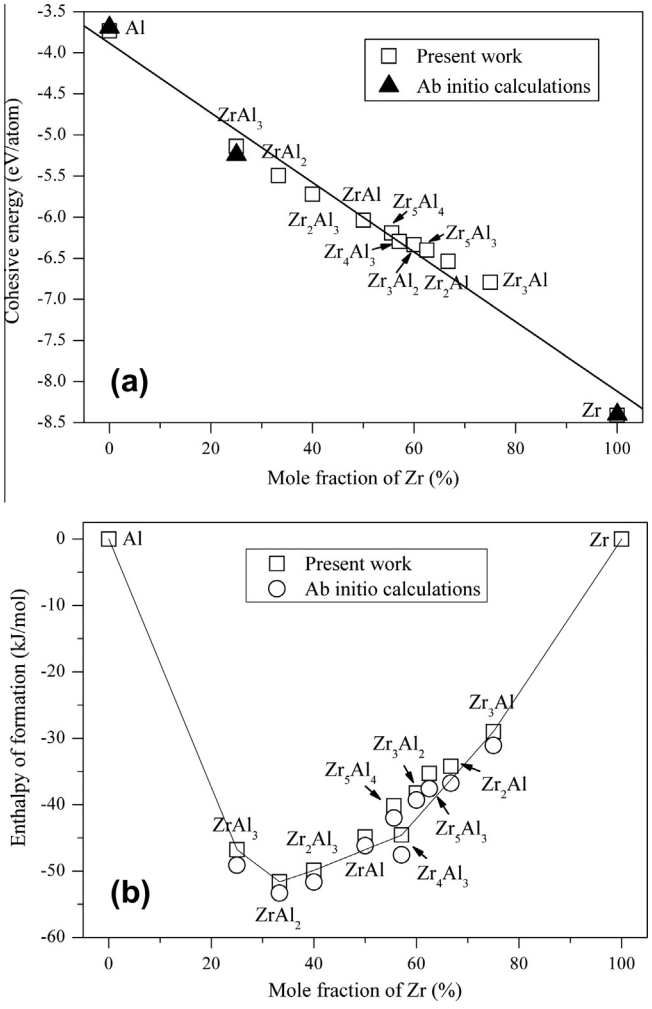

Fig. 3. Calculated cohesive energies (a) and enthalpies of formation (b) plotted as a function of mole fraction of Zr for the Zr–Al systems. The open circle denotes the data calculated by ab initio calculations.

lus can be used as a measure of the average bond strength of atoms for the given crystal [49,50]. As listed in Table 5, $ZrAl_2$ has the highest bulk modulus (112.46 GPa), while Zr_3Al possesses the lowest one (98.33 GPa). Therefore, $ZrAl_2$ has the strongest average bond strength of atoms and Zr_3Al has the lowest one. The shear modulus is the relationship between the resistance to reversible deformations and the shear stress [51,52]. A higher shear modulus G is mainly owing to a larger C_{44}. It is obviously that the largest C_{44} of $ZrAl_2$ (90.01 GPa) and the smallest C_{44} of Zr_5Al_4 (30.36 GPa) for considered intermetallic compounds result in the highest G of $ZrAl_2$ (90.22 GPa) and the lowest G of Zr_5Al_4 (45.94 GPa). The Young's modulus is defined as the ratio of stress and strain and can also be used as a measure of the stiffness of a solid. When the value of Young's modulus is large, the material is stiff [49,52]. In the present work, $ZrAl_2$ is stiffer than the other considered compounds due to its higher value of Young's modulus (213.55 GPa). Furthermore, a larger Young's modulus responds to the more covalent feature of the material [53]. It can be expected that the covalent bonding feature of $ZrAl_2$ is more dominant than that of other Zr–Al compounds.

The brittleness and hardness of the compounds are related to the value of B/G, that is, the compound with a smaller B/G value (<1.75) usually is brittle while the compound with a larger B/G value (>1.75) possesses ductile [54]. As another elastic parameter of compounds, Poisson's ratio v is consistent with B/G, which refers to ductile compounds usually with a large v (>0.26) [55]. Fig. 5 depicts the relationship among ductile or brittle properties, B/G and v. The values of B/G are larger than 1.75 and values of v are larger than 0.26 for Zr_5Al_4, Zr_3Al_2, Zr_5Al_3 and Zr_2Al in Fig. 5, which indicates that these four compounds are ductile. The other compounds in the Zr–Al binary system are brittle with their values of B/G and v smaller than 1.75 and 0.26, respectively. However, B/G and Poisson's ratios of the four ductile Zr–Al compounds are still less than pure Al and Zr, equally indicating that these intermetallics in Zr–Al system are relatively brittle and will reduce the ductility of Zr–Al alloys.

The universal elastic anisotropy index A^U for crystals with any symmetry is proposed as follow [56]:

$$A^U = 5\frac{G_V}{G_R} + \frac{B_V}{B_R} - 6 \geqslant 0 \tag{4}$$

In this equation, B_V (G_V) and B_R (G_R) are the bulk modulus (shear modulus) in the Voigt and Reuss approximations. A crystal with $A^U = 0$ means it is isotropic. The deviation of A^U from zero defines the extent of single crystal anisotropy and accounts for both the shear and the bulk contributions unlike all other existing anisotropy measures. Thus, A^U represents a universal measure to quantify the single crystal elastic anisotropy [56]. We constructed an elastic anisotropy diagram in the (B_V/B_R, G_V/G_R) space as shown in Fig. 6.

Table 4
The calculated elastic constants for Zr–Al intermetallic compounds in Zr–Al binary alloys.

Phase	Elastic constants (GPa)								
	C_{11}	C_{12}	C_{13}	C_{22}	$C_{23.}$	C_{33}	C_{44}	C_{55}	C_{66}
Al	107.66	61.17					28.93		
$ZrAl_3$	203.98	65.35	44.70			202.21	81.06		100.21
	208.8[a]	70.5[a]	49.1[a]			208.3[a]	87.2[a]		102.2[a]
$ZrAl_2$	236.81	46.65	57.05			217.22	90.01		
Zr_2Al_3	226.06	46.84	48.31	203.50	67.91	203.01	74.73	76.07	56.91
ZrAl	142.87	64.66	92.60	217.32	49.26	193.33	70.28	116.67	62.22
Zr_5Al_4	184.73	76.54	48.72			192.69	30.36		
Zr_4Al_3	218.20	40.11	57.23			213.16	74.62		
Zr_3Al_2	151.57	77.01	78.67			166.77	69.32		45.98
Zr_5Al_3	183.20	67.59	61.27			167.57	32.65		64.61
Zr_2Al	178.08	85.16	53.25			186.68	57.19		
Zr_3Al	146.45	74.27					75.67		
	163.8[b]	79.3[b]					86.5[b]		
α-Zr	152.73	55.75	65.39			161.74	26.23		45.25
	155.4[c]	67.2[b]	64.6[c]			172.5[b]	36.3[c]		44.1[c]

[a] Ref. [17].
[b] Ref. [43].
[c] Ref. [44].

Table 5
The calculated bulk modulus B (GPa), shear modulus G (GPa), Young's modulus E (GPa), B/G, Poisson's ratio v, anisotropic index A^U for Zr–Al intermetallic compounds in Zr–Al binary alloys.

	B	G	E	B/G	v	B_V/B_R	G_V/G_R	A^U	B [a]
Al	76.67	26.50	71.29	2.89	0.35	1.000	1.012	0.060	74.2
$ZrAl_3$	102.07	82.25	194.50	1.24	0.18	1.002	1.015	0.077	102.5
$ZrAl_2$	112.46	90.22	213.55	1.25	0.18	1.000	1.003	0.015	113.6
Zr_2Al_3	106.52	72.07	176.42	1.48	0.22	1.000	1.022	0.110	108.6
ZrAl	106.81	67.56	167.39	1.58	0.24	1.011	1.174	0.881	108.8
Zr_5Al_4	101.02	45.94	119.68	2.20	0.30	1.002	1.135	0.677	103.3
Zr_4Al_3	106.49	80.37	192.65	1.32	0.20	1.001	1.007	0.036	107.6
Zr_3Al_2	104.16	50.89	131.29	2.05	0.29	1.002	1.071	0.357	107.2
Zr_5Al_3	101.42	46.83	121.75	2.16	0.30	1.003	1.092	0.463	103.3
Zr_2Al	102.76	54.90	139.80	1.87	0.27	1.003	1.025	0.128	105.2
Zr_3Al	98.33	56.22	141.66	1.75	0.26	1.000	1.138	0.690	101.4
α-Zr	93.22	37.34	98.82	2.50	0.32	1.003	1.087	0.438	95.9

[a] Ref. [38].

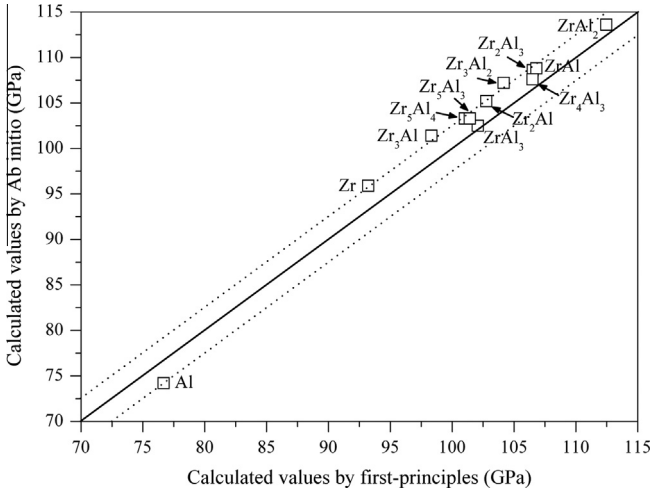

Fig. 4. Comparison of calculated bulk modulus in this work for the binary intermetallic compounds in the Zr–Al systems with the calculated values by ab initio calculations. The solid line shows unity ($y = x$) while the dotted lines present an error range of ±2.5 GPa.

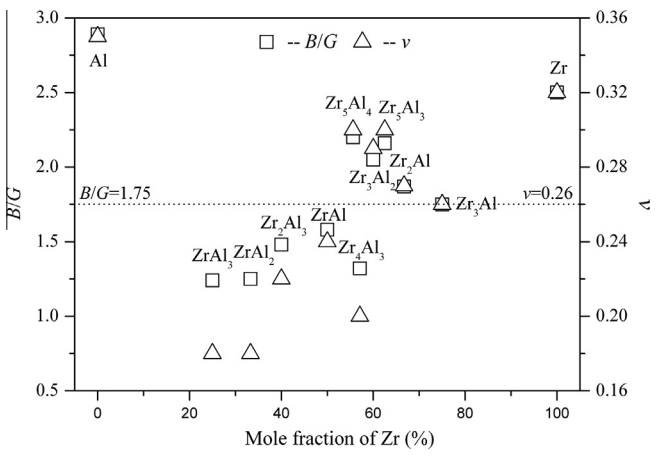

Fig. 5. The ductile/brittle properties of the Zr–Al binary compounds. The dotted line denotes the dividing line between ductile and brittle solids. Solids with $B/G > 1.75$ and $v > 0.26$ are ductile, the opposite are brittle.

Obviously, the region with $B_V/B_R \leqslant 1$ and $G_V/G_R \leqslant 1$ (i.e. $A^U \leqslant 0$) is not considered and no Zr–Al binary compounds lie here. The increment along the G_V/G_R axis affects the anisotropy A^U much more than along B_V/B_R axis because of the coefficient for G_V/G_R (=5) larger than that for B_V/B_R (=1). The larger A^U represents the more anisotropic. Although $ZrAl_2$ and Zr_2Al_3 belong to hexagonal and orthorhombic crystals, respectively, they are elastically similar to cubic crystal Zr_3Al with $B_V/B_R = 1$. Zr_3Al has a larger G_V/G_R of 1.138, and

Zr_3Al is more anisotropic than Zr_2Al_3 and $ZrAl_2$. For tetragonal structures $ZrAl_3$, Zr_3Al_2 and Zr_5Al_3, although their values of B_V/B_R are almost the same, the G_V/G_R for Zr_5Al_3 is 1.092 which is the largest in these three compounds. Therefore, Zr_5Al_3 is the most anisotropic, followed by Zr_3Al_2 and by $ZrAl_3$. One can draw the similar conclusion for hexagonal structures Zr_5Al_4, Zr_4Al_3 and Zr_2Al that Zr_5Al_4 has the most anisotropy due to the largest G_V/G_R (=1.135). It should be noted that the orthorhombic ZrAl with the largest A^U = 0.881 is the most anisotropic in Zr–Al binary compounds.

As a fundamental parameter for the solid's thermodynamic properties, Debye temperature (Θ_D) is related to specific heat, bond strength, elastic constants and melting temperature. The Debye temperature can be estimated from the average sound velocity by the following equation based on elastic constant evaluations [57]:

$$\Theta_D = \frac{h}{k}\left[\frac{3n}{4\pi}\left(\frac{N_A\rho}{M}\right)\right]^{\frac{1}{3}}\upsilon_m \tag{5}$$

where h is the Planck constant, respectively; N_A is the Avogadro number, M is the molecular weight, and ρ is the density. The average sound velocity υ_m can be calculated as follows [58]:

$$\upsilon_m = \left[\frac{1}{3}\left(\frac{2}{\upsilon_t^3}+\frac{1}{\upsilon_l^3}\right)\right]^{-\frac{1}{3}}, \quad \upsilon_l = \left[\left(B+\frac{4G}{3}\right)/\rho\right]^{\frac{1}{2}}, \quad \upsilon_t = \left(\frac{G}{\rho}\right)^{\frac{1}{2}} \tag{6}$$

where B and G are isothermal bulk modulus and shear modulus. υ_l is the longitudinal velocity and υ_t is the transverse sound velocity.

The calculated sound velocities and Debye temperatures Θ_D of Zr–Al compounds are tabulated in Table 6 compared with the other calculations and experiments. The values of sound velocities and Θ_D in cubic Al by calculation in this work are in good agreement with the other calculations and experiments. It is noted that the calculated Θ_D of $ZrAl_3$ (579 K) is very close to the experiment (577 K) [17] which is measured by the velocity of ultrasonic waves, and the value of Θ_D of $ZrAl_2$ in the present work is also in good agreement with the theoretical calculation [14]. There are no clear trends that can be observed from the data in Table 6 for the Zr–Al compounds: both the calculated values of sound velocity and Debye temperature scatter in a wide range. However, $ZrAl_3$ has a greatest Debye temperature in the considered Zr–Al compounds in the present work. As a rule of thumb, a greater Debye temperature means a larger associated thermal conductivity [14]. Therefore, $ZrAl_3$ should possess the best thermal conductivity relative to the other Zr–Al compounds.

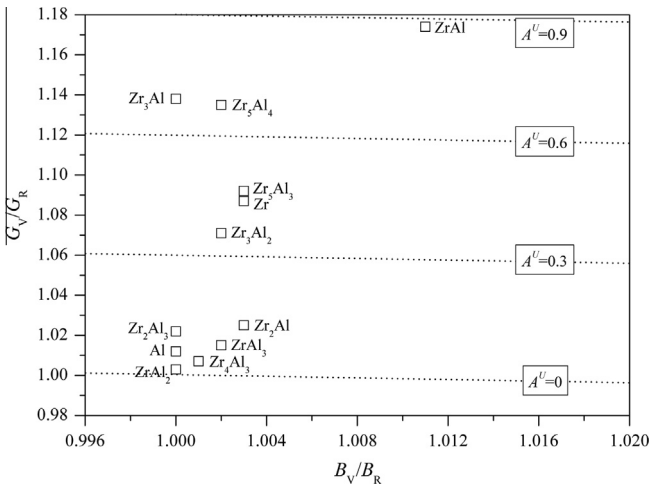

Fig. 6. The elastic anisotropy for the binary intermetallic compounds in the Zr–Al systems.

Fig. 7 shows the calculated enthalpies of formation (ΔH) compared with their shear modulus (G) and assessed congruent melting temperatures (T_m) of the Zr–Al intermetallics [8,62]. It is interesting to note that for the several compared compounds, the enthalpy of formation of a stable compound at 0 K is more negative if it has a higher melting temperature. This is to be expected since a more negative enthalpy of formation is an indicator of a greater stability and stronger interatomic bonding. Stronger bonding leads to higher melting temperature [63]. Such correlations between enthalpy of formation of solids and their melting temperatures have been observed experimentally in Mg–X binary systems (X = Ni, Dy, Y, Cd and La) [63] and $TiAl_3$ type compounds in the Al–Pt–Ti system [64]. The elastic modulus, especially shear modulus, is determined by the interatomic bonding of intermetallic, so the shear modulus is also concerned with the melting temperature which is higher melting temperature corresponding to larger shear modulus owing to the stronger interatomic bonding. For example, $ZrAl_2$ has the highest melting temperature than other Zr–Al compounds, and, as predicted, $ZrAl_2$ has the most negative enthalpy of formation and largest shear modulus from Fig. 7.

3.4. Electronic structures

The electronic energy band structures near Fermi level of the ten Zr–Al binary compounds considered in the present work have

Table 6
The density (in g/cm^3), elastic wave velocity (in m/s) and the Debye temperature (in K) for the polycrystalline compounds in Zr–Al binary alloys.

	ρ	v_l	v_t	v_m	Θ_D
Al	2.70	6196	3158	3539	413
		6127 [59]	3339 [59]	3725[59]	433 [59]
$ZrAl_3$	4.03	7248	4518	4978	571
		7332 [17]	4556 [17]	5022 [17]	577 [17]
$ZrAl_2$	4.52	7176	4468	4924	562
		7195 [14]	4413 [14]	4871 [14]	556 [14]
Zr_2Al_3	4.66	6594	3933	4353	488
ZrAl	4.97	6294	3687	4088	450
Zr_5Al_4	5.21	5581	2969	3318	364
Zr_4Al_3	5.34	6325	3880	4282	471
Zr_3Al_2	5.30	5697	3099	3457	376
Zr_5Al_3	5.40	5509	2945	3289	357
Zr_2Al	5.63	5591	3123	3476	378
					396 [60]
Zr_3Al	5.94	5401	3076	3419	369
					388 [43]
α-Zr	6.48	4698	2400	2689	280
					262 [43], 299 [61]

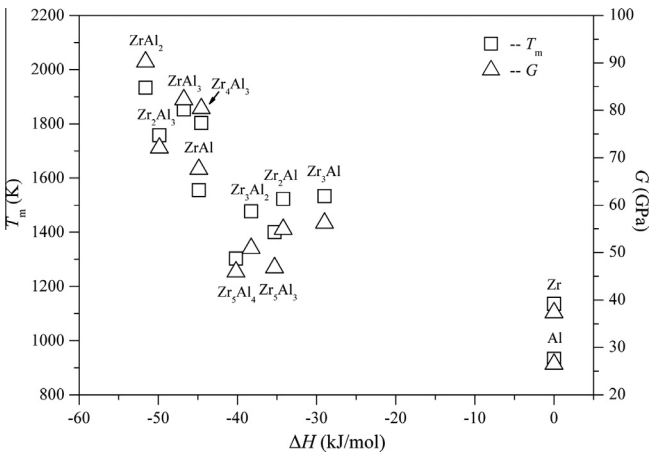

Fig. 7. Calculated enthalpies of formation of Zr–Al intermetallics compared with shear modulus and congruent melting temperature.

also been calculated and shown in Fig. 8. The zero energy means the Fermi level. It can be seen from Fig. 8 that the energies of band structures near Fermi level for these compounds are concentrated in the range of −10 to 5 eV. Four Zr–Al compounds, i.e. $ZrAl_2$, Zr_2Al_3, Zr_3Al_2 and Zr_5Al_3, have the band gaps which are 0.007 eV, 0.053 eV, 0.020 eV and 0.004 eV, respectively. For Zr_2Al_3, both the top valence band and the lowest conduction band are situated at $0.6 \times G - Y$ in Fig. 8. Therefore, Zr_2Al_3 is a direct band gap semiconductor. For $ZrAl_2$, Zr_3Al_2 and Zr_5Al_3, the valence band maximum and the conduction band minimum are located at different points, which indicate that $ZrAl_2$, Zr_3Al_2 and Zr_5Al_3 are indirect band gap semiconductors. As for other compounds considered in these ten Zr–Al compounds, their valence bands overlap the conduction bands at the Fermi surface in Fig. 8, and this demonstrates that all of them are conductors.

In order to gain further understanding of the basic features of the chemical bonding in Zr–Al binary compounds, the total density of states (TDOS) and partial density of states (PDOS) are investigated. Fig. 9 describes the TDOS and PDOS of Zr–Al binary compounds, and the energy zero is set as the Fermi level (E_F). The DOS shown in Fig. 9 reveal that, for these compounds, the part of TDOS below the Fermi level are mainly contributed by Al 3*p* and Zr 4*d* states, while the part of TDOS above the Fermi level are primarily contributed by Zr 4*d* states. It indicates that the 3*p* states of Al hybridize strongly with the Zr 4*d* states in the region below Fermi level, and atomic bonds would be formed between Al and Zr atoms.

In the PDOS, it is worth noting that the E_F of $ZrAl_2$ is exactly located at the pseudo-gap which is defined as the trough of *d* states. As a result, the maximum band-filling state is most easily reached in $ZrAl_2$ than the other compounds in the Zr–Al system, thus $ZrAl_2$ is the most stable compound. Moreover, the TDOS below the Fermi level for eight stable compounds at low temperatures in the Zr–Al binary system were also analyzed. It is found that the bonding electron numbers of these eight Zr–Al compounds per atom are 6.487 for $ZrAl_3$, 7.289 for $ZrAl_2$, 6.787 for Zr_2Al_3, 6.484 for ZrAl, 5.552 for Zr_4Al_3, 4.282 for Zr_3Al_2, 4.190 for Zr_2Al, and 3.745 for Zr_3Al between the Fermi level and −9 eV, respectively. Larger

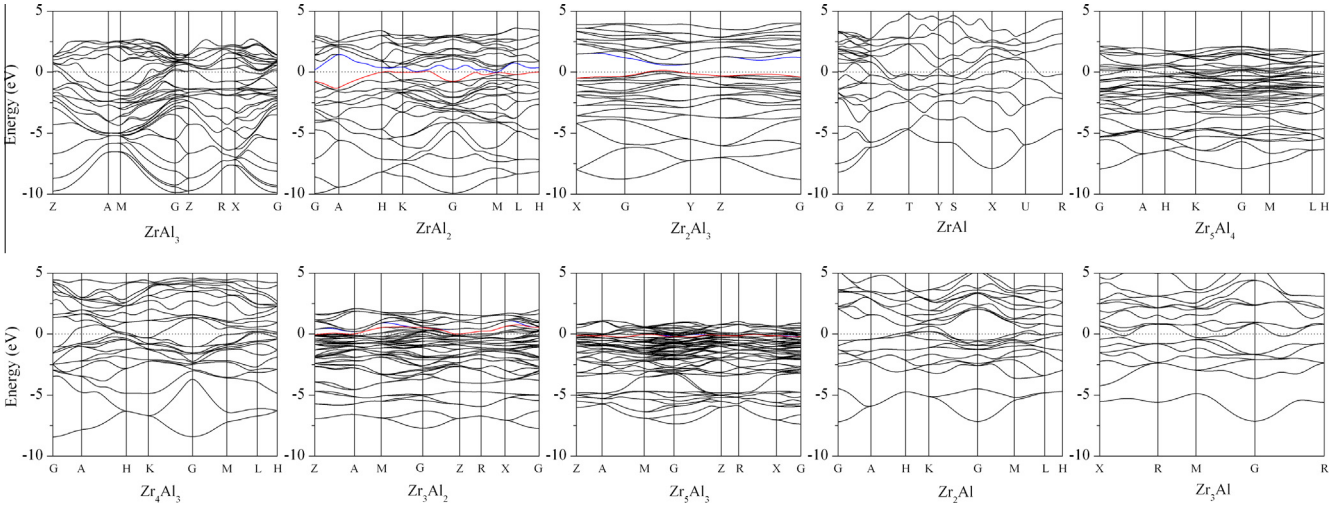

Fig. 8. The electronic energy band structures near Fermi level of Zr–Al intermetallic compounds. The dotted lines at zero energy denote the Fermi level E_F.

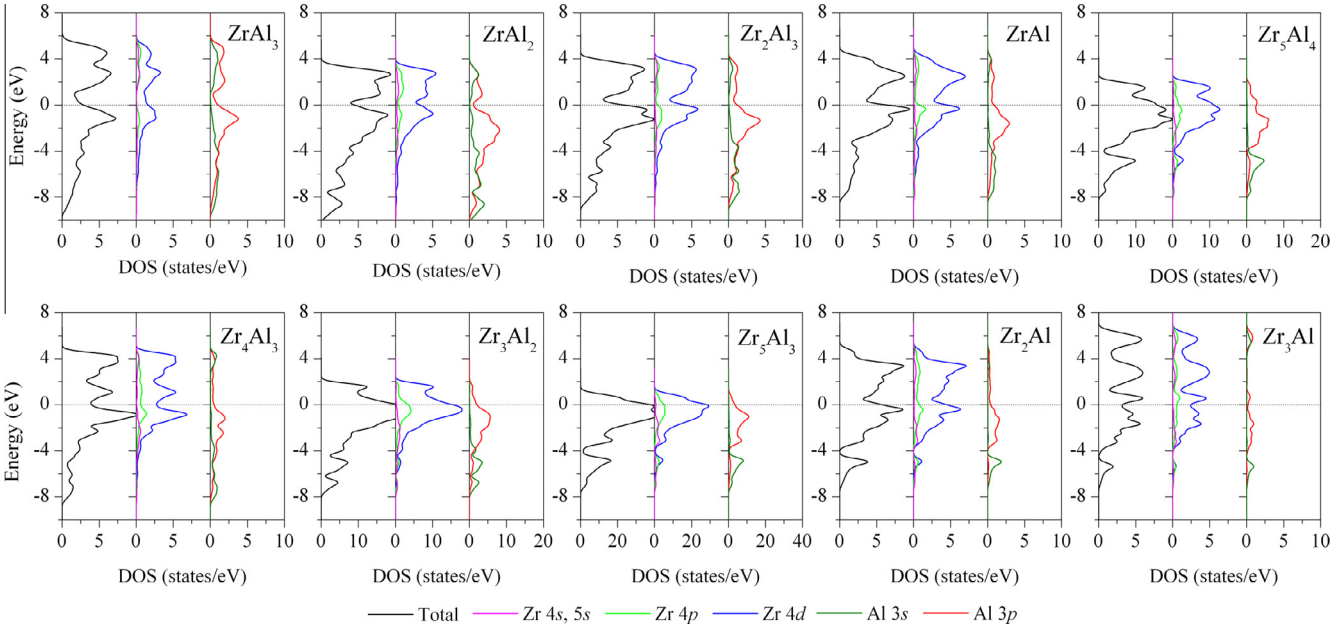

Fig. 9. Total and partial electronic densities of states near Fermi level of Zr–Al intermetallics. The dotted lines denote the Fermi level E_F.

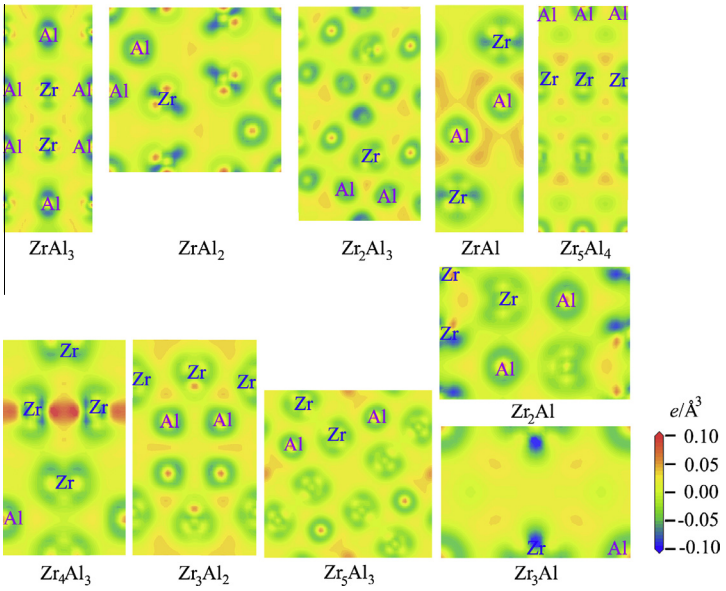

Fig. 10. The differences of charge density distribution for Zr–Al binary compounds in the (1 1 0) plane ($ZrAl_3$, $ZrAl_2$, Zr_5Al_4, Zr_4Al_3, Zr_3Al_2, Zr_2Al and Zr_3Al) and in the (0 0 1) plane (Zr_2Al_3, ZrAl and Zr_5Al_3). Electron excess is drawn in red and electron deficiency in blue. (For interpretation of the references to colour in this figure legend, the reader is referred to the web version of this article.)

Table 7
Atomic Mulliken charge and bond population analysis of stable Zr–Al binary compounds.

	Atom	s	p	d	Total	Charge (e)	Bond	Population	Length (Å)
$ZrAl_3$	Zr:4e	2.19	6.51	3.28	11.98	0.02	Al_{4c}–Zr	0.08	2.87
	Al1:4c	1.02	2.03	0	3.05	−0.05	Al_{4e}–Zr	0.21	2.85
	Al2:4d	1.04	2.00	0	3.04	−0.04			
	Al3:4e	1.05	1.88	0	2.93	0.07			
$ZrAl_2$	Zr:4f	2.31	6.34	2.94	11.59	0.41	Al_{2a}–Zr	0.40	2.70
	Ref. [14]	2.32	6.31	2.96	11.59	0.41			
	Al1:2a	1.05	2.11	0	3.16	−0.16	Al_{6h}–Zr	0.48	2.58
	Ref. [14]	1.05	2.11	0	3.15	−0.15			
	Al2:6 h	1.02	3.20	0	3.22	−0.22			
	Ref. [14]	1.02	3.20	0	3.22	−0.22			
Zr_2Al_3	Zr:16b	2.28	6.54	2.95	11.77	0.23	Al_{8a}–Zr	0.35	2.93
	Al1:8a	1.05	2.07	0	3.12	−0.12	Al_{16b}–Zr	0.13	2.91
	Al2:16b	1.05	2.11	0	3.17	−0.17			
ZrAl	Zr:4c	2.32	6.63	2.89	11.84	0.16	Al_{4c}–Zr	0.14	2.93
	Al:4c	1.04	2.11	0	3.16	−0.16			
Zr_5Al_4	Zr1:4d	2.35	6.64	2.90	11.89	0.11	Al_{2b}–Zr_{6g}	0.20	2.85
	Zr2:6 g	2.31	6.65	3.01	11.96	0.04	Al_{6g}–Zr_{6g}	0.23	2.93
	Al1:2b	1.09	1.97	0	3.06	−0.06			
	Al2:6 g	1.05	2.04	0	3.09	−0.09			
Zr_4Al_3	Zr1:2 h	2.33	6.49	2.99	11.82	0.18	Al_{3j}–Al_{3j}	0.49	2.72
	Zr2:1f	2.40	6.66	2.77	11.83	0.17	Zr_{2h}–Zr_{2h}	0.55	2.58
	Zr3:1b	2.40	6.66	2.77	11.83	0.17			
	Al:3j	1.04	2.20	0	3.24	−0.24			
Zr_3Al_2	Zr1:4d	2.42	6.67	2.71	11.80	0.20	Al_{8j}–Zr_{4g}	0.20	2.93
	Zr2:4f	2.32	6.66	2.88	11.86	0.14	Al_{8j}–Zr_{4f}	0.18	2.94
	Zr3:4 g	2.34	6.68	2.94	11.96	0.04			
	Al:8j	1.05	2.15	0	3.19	−0.19			
Zr_5Al_3	Zr1:4b	2.36	6.59	3.03	11.98	0.02	Al_{8h}–Zr_{4b}	0.26	2.88
	Zr2:16 k	2.37	6.66	2.83	11.86	0.14	Al_{4a}–Zr_{16k}	0.19	2.91
	Al1:4a	1.04	2.17	0	3.21	−0.21	Al_{8h}–Zr_{16k}	0.33	2.98
	Al2:8 h	1.05	2.14	0	3.19	−0.19			
Zr_2Al	Zr1:2a	2.38	6.63	2.89	11.89	0.11	Al_{2c}–Zr_{2d}	0.06	2.83
	Zr2:2d	2.32	6.68	2.98	11.98	0.02	Al_2–Zr_{2d}	0.22	2.96
	Al1:2c	1.03	2.10	0	3.13	−0.13			
Zr_3Al	Zr:3c	2.37	6.63	2.95	11.95	0.05	–	–	–
	Al:1a	1.02	2.11	0	3.14	−0.14			

bonding electron numbers correspond to the stronger charge interaction [65], and the phase stability of the compound will be better. Thus, $ZrAl_2$ has the best phase stability than others in the Zr–Al binary system.

For deeper insights into the differences of atomic bonding and electronic structures for these ten Zr–Al binary compounds, differences of charge density distribution are also investigated. Fig. 10 illustrates the differences of charge density distribution in the (1 1 0) plane for $ZrAl_3$, $ZrAl_2$, Zr_5Al_4, Zr_4Al_3, Zr_3Al_2, Zr_2Al and Zr_3Al, and (0 0 1) plane for Zr_2Al_3, ZrAl and Zr_5Al_3. Electron excess is characterized by red zone and electron deficiency is depicted as blue zone in units of number of electrons per $Å^3$. The charge density values in Fig. 10 are plotted from -0.1 e/$Å^3$ to 0.1 e/$Å^3$. The difference of charge density displays the polarization due to the formation of Zr–Al, Al–Al and Zr–Zr bonds.

For the transition metal–aluminum compounds, the main affecting factor of the enthalpy of formation is covalent bonds: more covalent bonds, more positive to the enthalpy of formation [66]. It is obvious from Fig. 10 that the covalent feature of Zr_3Al, with the minimal charge transfer between Zr and Al in Zr_3Al, is the least in these ten Zr–Al compounds. Thus, the enthalpy of formation of Zr_3Al is the largest one. For Zr_2Al, different from Zr_3Al, there are charges existing in the region between Zr atoms which indicating the Zr–Zr bonds mainly characterized by covalent. However, the charge transfer between Zr and Al is not significant in Zr_2Al. So the enthalpy of formation of Zr_2Al is only more negative than Zr_3Al. Although the charges transfer between Zr and Al in Zr_4Al_3 are not obvious, a large number of charges existing in the region between Zr atoms, showing stronger covalent features in Zr–Zr bonds. For the most stable phase $ZrAl_2$, the charge transfer occurs between each Zr atom and two Al atoms. The charge density around Zr atoms appears as a red two-petal shape in the (1 1 0) plane of $ZrAl_2$. This means that one Zr atom forms two covalent bonds with two Al atoms and $ZrAl_2$ mainly characterized by covalent, as a result, the enthalpy of formation is the most negative. The same result of the relationship between the enthalpy of formation and differences of charge density distribution for other compounds in Zr–Al system can be obtained according to Fig. 10.

Furthermore, the atomic Mulliken charge and bond population analysis of stable Zr–Al binary compounds are investigated, and the results are listed in Table 7. The results of atomic Mulliken charge population for $ZrAl_2$ are in good agreement with the other calculation by Hu et al. [14]. Table 7 clearly indicates that Al atoms gain electrons while Zr atoms loss electrons. The number of electrons transferred from Zr to Al in $ZrAl_2$ (1.64 *e*) is larger than that in the other Zr–Al compounds, indicating the bonding between Zr and Al in $ZrAl_2$ should be stronger than that in the other Zr–Al compounds. From Table 7, the calculated bond populations are positive in the considered Zr–Al compounds. It is clear that the Al–Zr bonds show strong covalent characters except Zr_4Al_3 and Zr_3Al. There are Al–Al and Zr–Zr covalent bonds in Zr_4Al_3. For Zr_3Al, due to the minimal charge transfer from Zr to Al, there are no Al–Zr bonds in the compound. The greater Al–Zr bond population (0.48) and smaller Al–Zr bond length (2.58 Å) in $ZrAl_2$ indicate that covalent interactions are stronger in $ZrAl_2$ than those in other Zr–Al compounds.

4. Conclusions

The structural properties, phase stability, elastic properties, band structures, densities of states, and differences of charge density distribution of the ten stable Zr–Al binary compounds have been investigated using first-principles methods based density functional theory in this work. It can be found that $ZrAl_2$ has the most negative enthalpy of formation and $ZrAl_2$ is the most stable. The results of elastic properties show that all of the ten compounds investigated in present work are mechanically stable, and the orthorhombic ZrAl is the most anisotropic in Zr–Al binary compounds. Zr_2Al_3 is a direct band gap semiconductor with the band gap of 0.053 eV. Furthermore, the differences of charge density distribution for Zr–Al binary compounds indicate that one Zr atom forms two covalent bonds with two Al atoms in the (1 1 0) plane of $ZrAl_2$ which leads to $ZrAl_2$ be the most stable compound in the Zr–Al system.

Acknowledgments

This work was supported by the National Natural Science Foundation of China under Grant No. 51201079, the Scientific Research Fund of Department of Education of Yunnan Province under Grant No. 2012Z099 and Scientific Research Foundation for Introduced Talents of KMUST under Grant No. KKSY201251033.

References

[1] E.M. Schulson, in: J.H. Westbrook, R.L. Fleischer (Eds.), Intermetallic Compounds, 2, John Wiley and Sons Ltd., New York, 1994.
[2] E.F. Ibrahim, B.A. Cheadle, Can. Metall. Q 24 (1985) 273.
[3] A. Laik, K. Bhanumurthy, G.B. Kale, Intermetallics 12 (2004) 69.
[4] H.W. Sheng, K. Lu, E. Ma, J. Appl. Phys. 85 (1999) 6400.
[5] Z. Fu, W.L. Jonson, Nanostruct. Mater. 3 (1993) 175–180.
[6] S. Gialanella, A.R. Yavari, R.W. Cahn, Scripta Metall. Mater. 26 (1992) 1233.
[7] E.M. Schulson, M.J. Stewart, Metall. Trans. B 7 (1976) 363.
[8] J. Murray, A. Peruzzi, J.P. Abriata, J. Phase Equilib. 13 (1992) 277.
[9] M. Ferrini, D. Gozzi, J. Alloys Comp. 317–318 (2001) 583.
[10] F. Willis, R.G. Leisure, I. Jacob, Phys. Rev. B 50 (1994) 13792.
[11] U. Anselmi-Tamburini, G. Spinolo, G. Flor, Z.A. Munir, J. Alloys Comp. 247 (1997) 190.
[12] M. Alatalo, M. Wienert, R.E. Watson, Phys. Rev. B 57 (1998) R2009.
[13] J. Belošević-Čavor, V. Koteski, B. Cwkić, A. Umićević, Comput. Mater. Sci. 41 (2007) 164.
[14] W.C. Hu, Y. Liu, D.J. Li, X.Q. Zneg, C.S. Xu, Comput. Mater. Sci. 83 (2014) 27.
[15] C. Colinet, A. Pasturel, J. Alloys Comp. 319 (2001) 154.
[16] C.S. Lue, B.X. Xie, S.N. Horng, J.H. Su, J.Y. Lin, Phys. Rev. B 71 (2005) 195104.
[17] M. Nakamura, K. Kimura, J. Mater. Sci. 26 (1991) 2208.
[18] R.M. Dreizler, E.K.U. Gross, Density functional theory: an approach to the quantum many-body problem, Springer, Berlin, 1990.
[19] M.H. Yoo, C.L. Fu, ISIJ Int. 31 (1991) 1049.
[20] A.E. Carlsson, P.J. Meschter, in: J.H. Westbrook, R.L. Fleischer (Eds.), Intermetallic Compounds, Vol.1, John Wiley and Sons Ltd., New York, 1994.
[21] M.D. Segall, P.J.D. Lindan, M.J. Probert, C.J. Pickard, P.J. Hasnip, S.J. Clark, M.C. Payne, J. Phys.: Condens. Matter. 14 (2002) 2717.
[22] J.P. Perdew, K. Burke, M. Ernzerhof, Phys. Rev. Lett. 77 (1996) 3865.
[23] H.M. Otte, W.G. Montague, D.O. Welch, J. Appl. Phys. 34 (1963) 3149.
[24] R.J. Kematic, H.F. Franzen, J. Solid State Chem. 54 (1984) 226.
[25] A. Israel, I. Jacob, J.L. Soubeyroux, D. Fruchart, H. Pinto, M. Melamud, J. Alloys Comp. 253 (1997) 265.
[26] T.J. Renouf, Acta Crystallogr. 14 (1961) 469.
[27] F.J. Spooner, C.G. Wilson, Acta Crystallogr. 15 (1962) 621.
[28] C.G. Wilson, D.K. Thomas, F.J. Spooner, Acta Crystallogr. 13 (1960) 56.
[29] C.G. Wilson, F.J. Spooner, Acta Crystallogr. 13 (1960) 358.
[30] L.E. Edsammar, Acta Chem. Scand. 14 (1960) 223.
[31] C.G. Wilson, D. Sams, Acta Crystallogr. 14 (1961) 71.
[32] M. Pötzschke, K. Schubert, Z. Metallkde 53 (1962) 548.
[33] H.H. Keeler, J.H. Mallery, J. Metals 2 (1955) 394.
[34] R.B. Russel, J. Appl. Phys. 24 (1953) 232.
[35] Y. Ma, C. Roemming, B. Lebech, J. Gjoennes, J. Taftoe, Acta Crystallogr. B 48 (1992) 11.
[36] R.V. Nandedkar, P. Delavignette, Phys. Stat. Sol. A 73 (1982) K157.
[37] N.J. Clark, E. Wu, J. Less-Common Met. 163 (1990) 227.
[38] G. Ghosh, M. Asta, Acta Mater. 53 (2005) 3225.
[39] S.V. Meschel, O.J. Kleppa, J. Alloys Comp. 191 (1993) 111.
[40] N. Saunders, Z. Metallkde 80 (1989) 894.
[41] T. Wang, Z. Jin, J.C. Zhao, J. Phase Equilib. 22 (2001) 544.
[42] Y.H. Duan, Y. Sun, M.J. Peng, Z.Z. Guo, Solid State Sci. 13 (2011) 455.
[43] E. Clouet, J.M. Sanchez, C. Sigli, Phys. Rev. B 65 (2002) 094105.
[44] E.S. Fisher, C.J. Renken, Phys. Rev. 135 (1964) 482.
[45] J.F. Nye, Physical Properties of Crystals, Oxford University Press, Oxford, 1985.
[46] B.B. Karki, G. Ackland, J. Crian, J. Phys.: Condens. Matter. 9 (1997) 8579.
[47] D.C. Wallace, Thermodynamics of Crystal, Wiley, New York, 1972.
[48] O. Beckstein, J.E. Klepeis, G.L.W. Hart, O. Pankratov, Phys. Rev. B 63 (2001) 134112.
[49] H. Ozisik, E. Deligoz, K. Colakoglu, G. Surucu, Chin. Phys. B 22 (2013) 046202.

[50] A.A. Maradudin, E.W. Montroll, G.H. Weiss, I.P. Ipatova, Theory of Lattice Dynamics in the Harmonic Approximation, Academic Press, New York, 1971.
[51] N. Korozlu, K. Colakoglu, E. Deligoz, S. Aydin, J. Alloys Comp. 546 (2013) 157.
[52] I.R. Shein, A.L. Ivanovskii, J. Phys.: Condens. Matter. 20 (2008) 415218.
[53] M. Rajagopalan, S. Praveen Kumar, R. Anuthama, Physica B 405 (2010) 1817.
[54] S.F. Pugh, Philos. Mag. 45 (1954) 823.
[55] J.J. Lewandowski, W.H. Wang, A.L. Greer, Philos. Mag. Lett. 85 (2005) 77.
[56] S.I. Ranganathan, M. Ostoja-Starzewski, Phys. Rev. Lett. 101 (2008) 055504.
[57] D. Music, A. Houben, R. Dronskowski, J.M. Schneider, Phys. Rev. B 75 (2007) 174102.
[58] J. Feng, B. Xiao, R. Zhou, W. Pan, D.R. Clarke, Acta Mater. 60 (2012) 3380.
[59] J. Feng, B. Xiao, C.L. Wan, Z.X. Qu, Z.C. Huang, J.C. Chen, R. Zhou, W. Pan, Acta Mater. 59 (2011) 1742.
[60] X.L. Yuan, D.Q. Wei, Y. Cheng, Q.M. Zhang, Z.Z. Gong, J. At. Mol. Sci. 3 (2012) 160.
[61] R. Bechmann, R.F.S. Hearmon. in: Landolt-Börnstein, K.-H. Hellwege, A.M. Hellwege (Eds.), vol. III/1, Springer, Berlin, 1966.
[62] T. Shindo, Y. Waseda, A. Inoue, Mater. Trans. 43 (2002) 2502.
[63] H. Zhang, S.L. Shang, J.E. Saal, A. Saengdeejing, Y. Wang, L.Q. Chen, Z.K. Liu, Intermetallics 17 (2009) 878.
[64] Y.H. Duan, Y. Sun, L. Lu, Comput. Mater. Sci. 68 (2013) 229.
[65] C.L. Fu, X. Wang, Y.Y. Ye, K.M. Ho, Intermetallics 7 (1999) 179.
[66] Y.G. Zhang, Y.F. Han, G.L. Chen, J.T. Guo, X.J. Wan, D. Feng, Structural Intermetallics, National Defence Industry Press, Beijing, 2001.